Self-Assembled Biconvex Microlens Array Using Chiral Ferroelectric Nematic Liquid Crystals

Kelum Perera[1,2], Arwa Alyami[1,2], Alex Adaka[2,3], Md Sakhawat H. Himel[2,3], Nilanthi Haputhantrige[1,2], Oleg D. Lavrentovich[1,2], Elizabeth Mann[1,2], and Antal Jákli[1,2,3]

[1]Department of Physics, Kent State University, Kent OH, 44242, USA
[2]Advanced Materials and Liquid Crystal Institute, Kent State University, Kent OH, 44242, USA
[3]Materials Science Graduate Program, Kent State University, Kent OH, 44242, USA

Abstract

Recently, it has been shown (Popov et al, Sci. Rep, 2017, 7, 1603) that chiral nematic liquid crystal films adopt biconvex lens shapes under water, which may explain the formation of insect eyes, but restricts their practical application. Here we demonstrate that chiral ferroelectric nematic liquid crystals, where the ferroelectric polarization aligns parallel to the air interface, can spontaneously form biconvex lens arrays in air when suspended in submillimeter-size grids. Using Digital Holographic Microscopy, we show that the lens has a paraboloid shape and the curvature radius at the center decreases with increasing chiral dopant concentration, i.e., with decreasing helical pitch. Simultaneous measurements of the imaging properties of the lenses show the focal length depends on the pitch, thus offering tunability. The physical mechanism of formation of the self-assembled ferroelectric nematic microlenses is also discussed.

Keywords: *Chiral ferroelectric nematic, Microlens array, geometric optics*

1. Introduction

Flat liquid crystal microlens arrays (LC-MLAs) [1–3] can capture the depth of field by tuning their focal length by applying non-uniform electric field via patterned electrodes. However, the non-uniform electric field leads to formation of disclination lines, which reduces image quality. Toric focal conic domains (TFCDs) formed in patterned surfaces in SmA liquid crystals have been shown to also function as MLAs [4,5]. They can be polymer stabilized even in their nematic phase where they can be electrically tuned with uniform field applied between ITO coated substrates [6]. All the above examples used flat liquid crystals.

Liquid crystal lenses with curved surfaces were observed recently when it was found that chiral nematic liquid crystals suspended in submillimeter size hexagonal grid arrays spontaneously form biconvex lens arrays when immersed in water [7,8]. Similar to the insects' compound eyes, the focal lengths of such lenses depend on the polarization state of the light. This observation implies that the compound eyes of insects such as bees, dragonflies, and certain beetles [9–12] which made up of chiral chitin, have a structure analogous to that of chiral nematic liquid crystals [13]. Additionally, it was found that such self-assembled lenses require that the liquid crystal director should be parallel to the interface, as is true in water. Since in most nematic liquid crystals the director aligns perpendicular to the air interface, lens formation of chiral nematic liquid crystals is generally not possible in air. This motivated us to find a way to develop self-assembled biconvex liquid crystals lens arrays in air. As a first step, we recently demonstrated that polarization-dependent plano-concave lens arrays of polymer stabilized chiral nematic liquid crystals can be produced in air [14] and could be even tuned by in-plane electric fields [15] when such lenses were made from chiral ferroelectric nematic (N_F^*) liquid crystals [16–20]. The advantage of the recently discovered ferroelectric nematic (N_F) liquid crystals [21–26] is the sensitivity to low fields due to their large ferroelectric polarization ($P_o \sim 50\ mC/m^2$) [22,24,27], and possibly large dielectric anisotropy [17– 19]. An additional important feature of the N_F materials is that they align parallel to the liquid crystal air interface [28] due to the depolarization field $\vec{E}_{dep} = -\frac{\vec{P}}{\varepsilon_o \varepsilon}$ that exerts a torque on the director until it turns parallel to the insulating surface. The effect of chirality in ferroelectric nematic liquid crystals (N_F^*), obtained using either via slight chiral modifications [16,20] or through doping by non-polar chiral compounds [17,18,29], have been also studied recently [16–20]. The resulting structure is twisted, just as in ordinary cholesterics, but with locally polar order.

Motivated by the above results, here we present studies on spontaneously formed bi-convex lens arrays of ferroelectric nematic liquid crystals when suspended in submillimeter size grids. We show that, while the pure ferroelectric nematic material forms a biconvex lens with a dent in their center, chiral ferroelectric nematic materials form paraboloid shape biconvex lenses without a dent. The shape and the focal length of these N_F^* lenses depend on the concentration of the chiral dopant and are independent of the polarization of the incoming light.

2. Experimental Results

For our studies we have used a room temperature ferroelectric liquid crystal mixture, FNLC 919 from Merck. On cooling it has two nematic phases N and N_1 above the N_F phase with the phase sequence $I\ 80°C\ N\ 44°C\ N_1 32°C\ N_F\ 8°C\ Cr$. FNLC 919 was studied by Yu et al [30] and Máthé et al [31,32]. It has a ferroelectric polarization at room temperature of $P_o \approx 4.7 \cdot 10^{-2} C/m^2$ [32] .

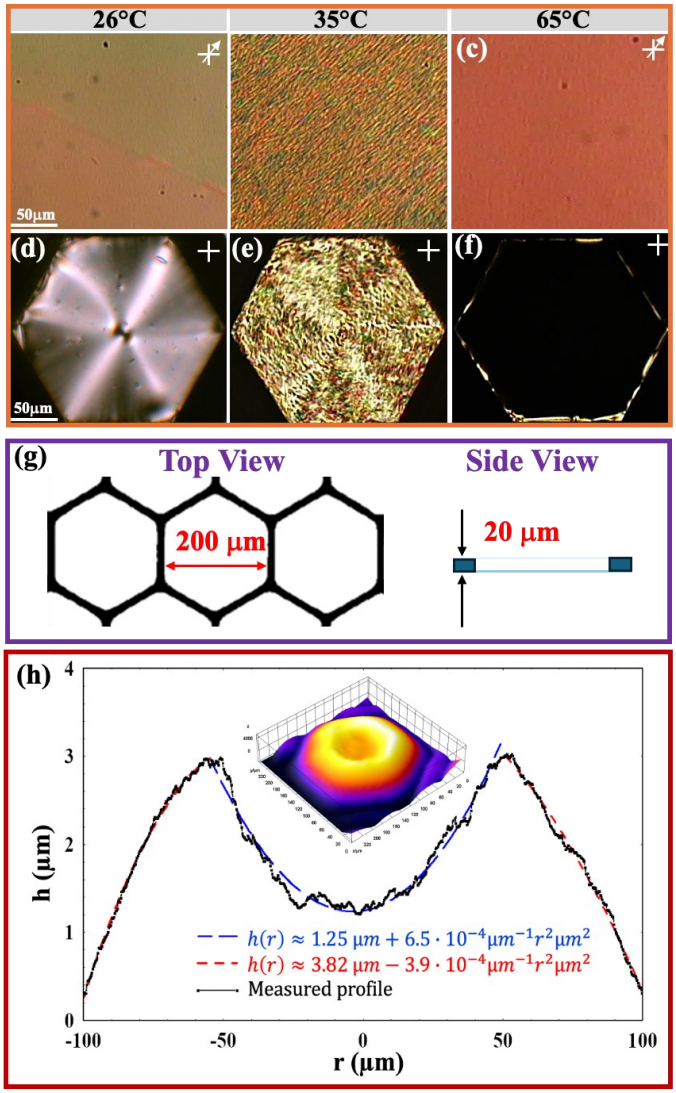

Figure 1: Properties of FNLC 919 in films and suspended in grids. (a-c): POM images of a 10.3 µm FNLC 919 film between unidirectionally rubbed planar cell. (a): N_F phase at 26°C, (b): N_1 phase at 35°C, (c): N phase at 65°C (c). (d-f): FNLC 919 suspended in a TEM grid at the same temperatures as in (a-c), respectively. White crosses show the direction of the crossed polarizers and white arrow indicates the rubbing direction. (g): Schematic illustration of the TEM grid.(h):2D surface profile of the cross-section cut through the center of one grid, measured by Digital Holographic Microscopy (DHM) from Lyncée Tec. Inset shows the 3D surface profile.

The textures in the different liquid crystal phases of a 10.3 μm FNLC 919 film between unidirectionally rubbed planar cell are shown in Figure 1(a-c). In the N_F, and the high temperature N phase, the textures are uniform. The intermediate N_1 phase, similar to twist-bend nematic phases [33], shows stripes along the rubbing direction (see Figure 1(b)) with a periodicity of $p{\sim}5\ \mu m$.

Typical textures are shown in Figure 1(d-f) for FNLC 919 suspended in $50/100$ mesh nickel double grids from Ted Pella, Inc. with mesh size of $200\ \mu m$ and thickness of $d = 20\ \mu m$ (see schematics in Figure 1(g)) designed for transmission electron microscopy (TEM) measurements. The texture in the higher temperature range of the N phase (Figure 1(f)) is completely dark between crossed polarizers, marking homeotropic alignment with the director uniformly normal to the substrates. This is typical for most rod-shaped nematic materials at the air interface. Cooling the material to the N_1 phase (Figure 1(e)), the texture brightens, and concentric stripes are seen, showing tangential director structure. These tangential stripes indicate that the N_1 phase is locally polar, so that in adjacent stripes the polarization is likely opposite such as in the splay nematic phase proposed by Mertelj et al [34] and in the antiferroelectric smectic Z_A phase found by Chen et al [35]. In the N_F phase (see Figure 1(d)) a defect, similar to that which has been reported both in sessile droplets [36] and in FNLC droplets in their isotropic melt [37,38], is seen at the center. Around the defect line running perpendicular to the film surface, the director profile is tangential to avoid the creation of a depolarization field [28,39]. Additionally, we can see faint (bluish) circular interference fringes indicating curved surfaces.

Figure 1(h) shows the shape measured with Digital Holographic Microscopy (DHM) of FNLC 919 suspended in a hexagonal TEM grid at room temperature. The main pane shows the shape of cross-section cut through the center of the grid. One can see that the film has increasing height toward the center, until, at about 50 μm from the center, the thickness decreases with an indentation at the middle. The dent is $\sim 1.75\ \mu m$ deep and $\sim 100\ \mu m$ wide. Its shape could be fitted by a parabola as shown by dotted blue line. The equation of the best fit is shown in the legend. The outer areas could be also fitted by a downward parabola (red dotted lines) with equation also shown in the legend. We note that the outer areas could also be fitted with circular segment of $R{\sim}1.3\ mm$ radius, but that fit was slightly worse than for the parabola. The inset in Figure 1(g) is the 3D

rendering of the surface profile, showing radial symmetry of the top view, corresponding to paraboloid shapes of both the rim and the dent areas.

Next, we studied the effect of chiral dopant and the addition of a conventional non-ferroelectric nematic material pentyl cyano biphenyl (5CB) on the director alignment and of the shape of FNLC 919 films suspended in hexagonal grids. Figure 2(a-c) shows typical textures of FNLC 919 doped with 2wt% S 811 from Merck at 26 °C, 35 °C and 65 °C, respectively.

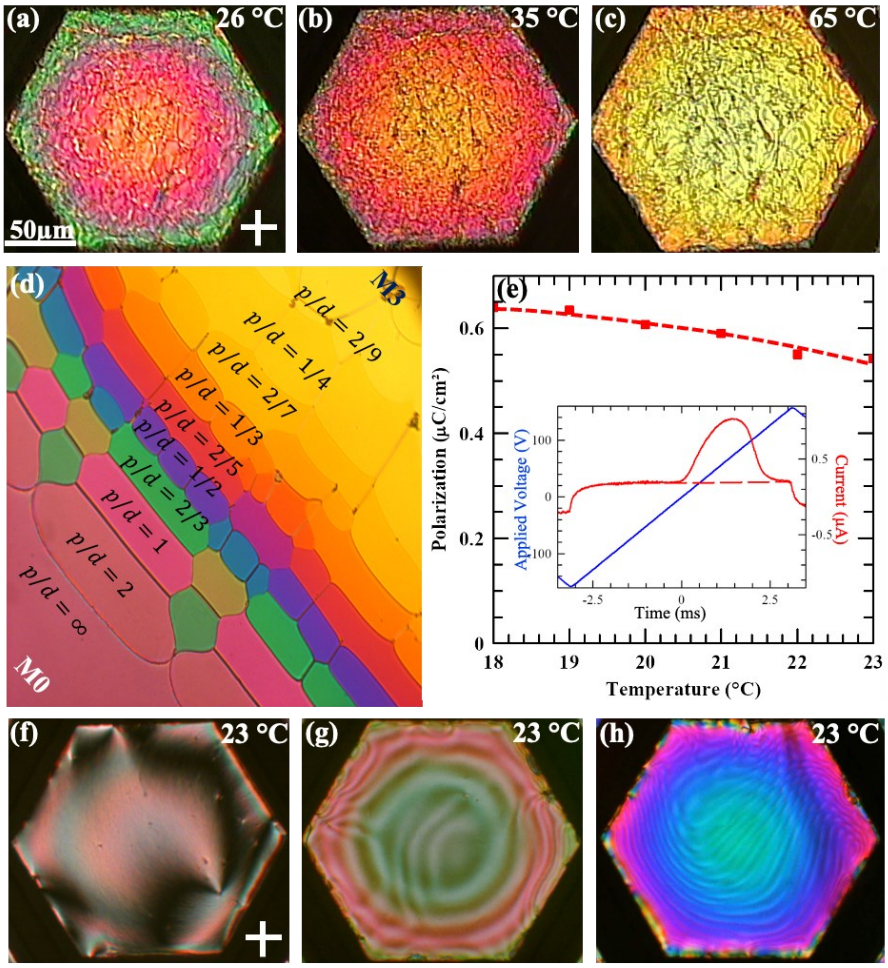

Figure 2: Summary of the results on FNLC 919 mixed with 2wt % chiral dopant S 811 and mixtures M0 (FNLC 919 + 10 wt % 5CB) and MX (M0 +X wt% S 811). (a-c): POM images of chiral FNLC 919 suspended in a TEM grid at 26 °C, 35 °C and 65 °C, respectively. White cross in (a) shows the direction of the crossed polarizers. (d): POM image of a 10.3µm contact cell filled with M0 from the bottom left and with M3* (FNLC 919+3 wt.% S811) from the top right corner. The bands with different colors correspond to varying helical pitch that decreases from infinity at 0% S811 to p=2d/9=2.3µm at 3 wt.% S811. (e): Temperature dependence of the spontaneous polarization of M0 measured using in-plane 80 Hz triangle wave voltages in* $10.9\ \mu m$ *thick planar cell with* $0.5\ mm$ *electrode gap. Inset: time dependence of the polarization current and of the applied voltage. (f-h): POM images of M0 (f), M1* (g) and M4* (h) suspended in grids at* $23\ °C$.

In the N_1^* and N_F^* [17,18] phases oily streak defects appear in Figure 2(a,b) similar to those in short-pitch chiral nematic (cholesteric) phases while in the *N* phase, Figure 2(c) the chiral mixture shows fingerprint texture corresponding to homeotropic surface alignment. Importantly, in the N_F^* phase the central defect seen in the N_F disappeared. In the high-temperature range of the N^* phase the birefringence color indicates basically uniform thickness. The textures in the N_1^* phase, and even more in the N_F^* phase, show systematic radial variation of the birefringence color from the edge to the center, indicating a radial biconvex lens-shape variation in the thickness. The underlying assembly mechanism is very similar to that Popov et al reported for N* under water [7]. Basically, it is related to the decrease of the free energy by reducing the contact area with the side walls of the grid where the helical structure unwinds. The material self-assembles into a lens shape to minimize the free energy of the system. Unfortunately, unlike in normal N^* materials under water, the oily streaks do not disappear quickly but stay for a long time (hours) and lead to light scattering that would reduce the image quality of such lenses. The oily streaks persist even under slower (0.5 °C/min) cooling rate, indicating high viscosity.

In order to decrease the viscosity while preserving the planar alignment, we added 10 wt% of commercially available LC, 4′-Pentyl-4-biphenylcarbonitrile (5CB) ($\Delta n \sim 0.2$, $\Delta\varepsilon \sim 10$, Merck) to FNLC 919 and denote the mixture as M0. Two chiral mixtures M1* and M4* were prepared by adding 1 wt% and 4 wt% chiral dopant S811 to M0, respectively. To measure the pitch, we prepared $d = 10.3\mu m$ thick contact cell between M0 and M3* as shown in Figure 2(d). One can see 9 bands corresponding to regions with decreasing pitch from infinite at M0 to $p = 2d/9 = 2.3\mu m$ at M3*. From this we can calculate that the helical twisting power (HTP) of S811 in M0 is $HTP = \frac{1}{c \cdot p} = \frac{1}{0.03 \cdot 2.3\ \mu m} = 14.5\ \mu m^{-1}$. Knowing the HTP of S811, we calculate the pitch of M1* and M4* as $p \sim 6.9\ \mu m$ and $p \sim 1.7\mu m$, respectively.

Figure 2(e) shows the temperature dependence of the polarization measured for M0 applying $80\ Hz$ in-plane triangle wave voltages in a $10.9\ \mu m$ thick planar cell with $0.5\ mm$ electrode gap. The value of the ferroelectric polarization P was calculated from the integral area of the current $\dot{Q}_P$ above the dotted red line shown in the inset as $P = \frac{\int \dot{Q}_P dt}{2A}$, where A is the cross sectional area normal to the polarization vector and $Q_P = P \cdot A$ is the polarization charge accumulated at the in-plane electrodes [27,40].

At 23°C where M0 transitions to the N_F phase, the value of the polarization was found to be $P\sim$ 0.6 μC/cm^{-2}. This value is 7 times smaller than the value we measured for FNLC 919 [32].

In accordance with the ferroelectric nature of M0 at room temperature, Figure 2(f) shows that M0 has planar anchoring, but without any defect in the center. The POM textures of M1* and M4* in Figure 2(g, h) show concentric interference rings with simultaneous radially increasing optical path difference ($\Gamma = \Delta n \cdot D(r)$, where Δn is the birefringence and $D(r)$ is the thickness of the lens) toward the center of the grid. The concentric rings are due to the interference between the liquid crystal film and the air [41], the number of fringes m that separate areas with a thickness difference of one wavelength λ can be also used to estimate the variation of the film thickness as $\Delta D \sim m \cdot \lambda$, where $\Delta D = D(0) - D(a)$ is the difference of the film thickness at the center and at the periphery of the film. As can be seen in Figure 2(g, h), $m \approx 4$ for M1* and $m \approx 8$ for M4*, indicating that film thickness variation is larger for higher chiral dopant concentration.

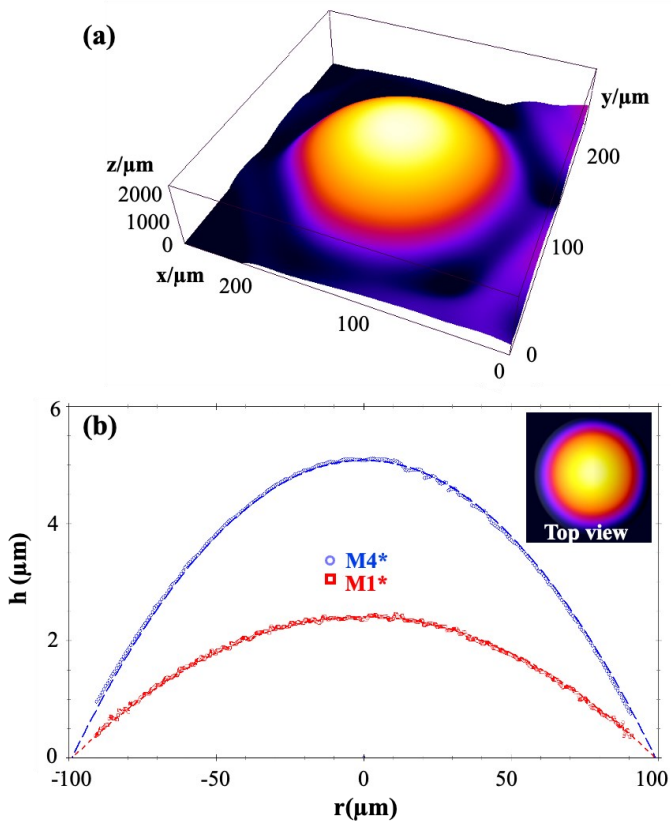

Figure 3: The height profile as a function of distance from the center of lenses using M1 and M4* mixtures. (a) 3D profile of M1*. (b) The radial dependence of the height at the cross-section through the center. Inset: top view of M1*.*

To quantify the top surface profile of the microlens, we measured the surface profile of the microlens using DHM. The height profile of the lenses as a function of distance measured from the center r using M1* and M4* mixtures are shown in Figure 3. Figure 3(a) shows the 3D rendering of the height profile of M1*. The radial dependence of the height at the cross-section through the center of M1* and M4* are shown in Figure 3(b) with the top view of M1* in the inset. It is found that the top surface has a parabolic profile with $h(r) = h(0)(1 - r^2/a^2)$ function, where $a \gg h(0)$ is the radius of the lens aperture. The radius of the curvature at the center of the lens can be calculated as $R = \frac{h(0)}{2} + \frac{a^2}{2 \cdot h(0)} \approx \frac{a^2}{2 \cdot h(0)}$ and the focal length $f = \frac{a^2}{2(n_{LC}-1)h(0)} \approx \frac{R}{(n_{LC}-1)}$ [42]. Best fits gave $h(0) = 2.46\ \mu m$ for M1* and $h(0) = 5.18\ \mu m$ for M4*. From these the radii of curvature for the M1* and M4* lenses are $R(1) \approx 2.03\text{mm}$ and $R(4) \approx 0.97$ mm. Approximating the birefringence as $\Delta n = n_{\parallel} - n_{\perp} \approx 0.2$ and $n_o = n_{\perp} \approx 1.52$, due to the planar alignment $n_{LC} \approx n_{\parallel} \sim 1.72$, which give $f \sim 2.8\ mm$ and $f \sim 1.34\ mm$ for the M1* and M4* lenses, respectively.

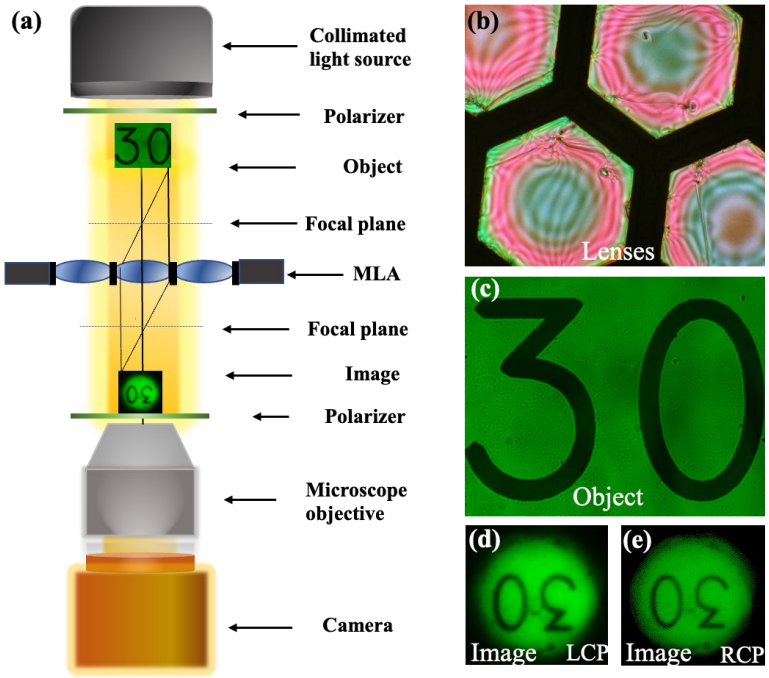

Figure 4: Optical setup and polarized optical microscopy (POM) image of the microlens array fabricated with M1 viewed between crossed polarizers. (a): Optical setup to measure the image and object distances. (b): Microlens array created with M1* (c): Object "30" written on the microscope calibration glass slide. (d): Image created by one of the microlenses using left circularly polarized light (LCP). (e) Image created by one of the microlenses using right circularly polarized light (RCP).*

We also determined the focal lengths of the microlenses directly by measuring the object and image distances (o and i, respectively) of the lenses that give $f = \frac{o \cdot i}{i+o}$. For this, we used an Olympus CK40 inverted polarizing optical microscope (POM) equipped with A QICAM Fast1394 CCD camera as illustrated in Figure 4(a), and focused first on the lenses (Figure 4(b)), then on the Object "30" (Figure 4(c)) and finally, on the inverted image (Figure 4(d,e)).

Independently, for M1* we measured $i = 4.8\,mm$ and $o = 8.9\,mm$, which provides $f = 3.1\,mm$, regardless of the polarization state of the incoming light. This is close to the value calculated from the measured shape. For the M4* mixture, the same object distance provided $i = 1.8\,mm$ image distance giving $f = 1.5\,mm$, which is also close to the calculated values based on the shape.

3. Discussion

The main goal of this work was to obtain self-assembled bi-convex liquid crystals microlens array in air by using ferroelectric nematic liquid crystals that provide planar alignment at the LC-air interface. During the process of this development, we have observed unforeseen shape with a central dent of the pure ferroelectric nematic liquid crystal mixture, FNLC 919. Before discussing the main focus of the paper, we attempt to explain the formation of this shape. As shown in Figure 1(g), the self-assembled shape of the N_F material can be best fitted by an outside convex and an inside concave paraboloid shape. The dent in the center of the film is likely related to the central defect line that connects positive and negative bound charges near the surface of the film as was discussed for pancake shaped N_F domains in their isotropic melt [39]. The depression may be explained by the equilibrium between the attractive electrostatic force F_E between the bound charges and the capillary force F_C acting on the defect that ends at the surface. The electrostatic force can be written as $F_E = \frac{q^2}{4\pi\varepsilon_o L^2}$, where $q = \iiint \vec{\nabla} \cdot \vec{P} dV \sim V \cdot \left|\vec{\nabla} \cdot \vec{P}\right| \sim \left|\vec{\nabla} \cdot \vec{P}\right| \cdot l^3 \sim P l^2$. Here we approximated the volume V of the polarization splay as l^3, where l is the diameter of the defect line. As the depth of the depression is much smaller than the thickness $D = 20\ \mu m$ of the grid, we also use the approximation that the distance between of the polarization charges is $L \sim D = 20\ \mu m$. The capillary pressure can be written as $p_C = \frac{2\gamma}{R}$, where $\gamma \sim 3 \cdot 10^{-2} N/m$ is the surface tension of the liquid crystal, and R is the curvature radius of the depression at the center. For parabolas we

can write that $R = \frac{b^2}{2g}$, where $b{\sim}50\ \mu m$ is the radius and $g{\sim}1.25\ \mu m$ is the depth of the depression. Since the depression is shallow ($b \gg g$), the capillary force can be approximated as $F_C \approx \frac{2\gamma}{R} \cdot b^2\pi$.

With these, at equilibrium we can write $\frac{(Pl^2)^2}{4\pi\varepsilon_o D^2} \approx \gamma g\pi$, and we can express the unknown diameter of the defect as $l \approx \sqrt[4]{\frac{4\gamma g\pi^2\varepsilon_o D^2}{P^2}} \sim \left(\frac{4{\cdot}3{\cdot}10^{-2}{\cdot}1.25{\cdot}10^{-6}\pi^2{\cdot}8.85{\cdot}10^{-12}{\cdot}4{\cdot}10^{-10}}{2.5{\cdot}10^{-3}}\right)^{\frac{1}{4}} {\sim}10^{-6}\ m{\sim}1\ \mu m$. This is a reasonable diameter for a +1 disclination that escape to the third dimension by twist. In spite of this reasonable estimate, this model should be tested with respect to the screening effect of free ions, which is out of the scope of this paper.

We note that depressions near defects of liquid crystal films with free surfaces have been known and understood for nematic [43–45] and smectic [46] liquid crystals, and for liquid crystal elastomers [47]. Typically, the dents are sharp when the defect lines cross the surface and shallower (just in our case), when they end inside the film [45] indicating that in FNLC free-standing films the defect is also confined inside the film. In all the above examples, however the free surface is flat far away from the defect. In contrast to this, in our case we find that the film has a convex paraboloid shape outside the defect area. This might indicate a spontaneous chiral structure of the ferroelectric nematic materials between degenerate planar anchoring as has indeed been observed for other ferroelectric nematic liquid crystals between planar and degenerate planar substrates [48].

The biconvex shape observed in the N_F^* phases of FNLC 919 and its diluted mixtures is similar to those observed by Popov et al in N* materials under water [7]. This is because the N_F material has planar alignment at the air-LC interface. In spite of this similarity, we have two notable features that require explanation.

(i) In contract to the spontaneously chiral N_F material without chiral dopant, we do not see the depression in the center. This is either due the absence of the defect line, or because the defect line is thinner than can be optically resolved in the POM textures in Figure 2 (a and f-g) and does not lead to depression of the surface. This latter situation could be the result of the almost one order of magnitude lower ferroelectric polarization of M0 that of the pure FNLC 919. Such a small polarization splay charge could be screened by free ions present in the sample, thus avoiding electrostatic attraction.

(ii) In contrast to the observations by Popov et al in N* materials under water [7] and to self-assembled plano-convex lenses [14], the focal length of the N_F^* lens is independent of the polarization state of the incoming light. This indicates that the ferroelectric nematic liquid crystal lens does not have Panchnarathnam-Berry (PB) phase properties. In the previous N* samples PB phase properties originated in the varying film thickness and the uniform pitch which resulted in a radially varying director structure at the surfaces. The absence of the radially varying director profile on our N_F^* materials can be understood as a result on the tangential director profile at the surface and the addition of the spontaneous chirality to chiral dopant dictated uniform chirality.

In summary, we showed that, similarly to our previous studies of chiral nematic microlenses formed under water [7], the addition of chiral dopants to ferroelectric nematic liquid crystals leads to the formation of microlenses when suspended in sub-millimeter size grids in air. This verifies that the combination of chirality and planar alignment of the liquid crystal at its surfaces leads to lens formation. Therefore, we can fabricate chiral ferroelectric nematic microlenses in air, enabling their use in a wide range of optical applications such collimation of lasers diodes, illumination systems, imaging systems and sensors. These results represent a significant improvement compared to the biconvex microlens arrays formed in the presence of water as our lenses work in air. This advance is thanks to the newly discovered ferroelectric nematic liquid crystals that have planar alignment at air interfaces.

Additionally, our results reveal a self-assembled paraboloid shape with a central depression of the non-chiral ferroelectric nematic film suspended in a grid, which is likely related to a spontaneously chiral polar structure.

4. Acknowledgement

This work was financially supported by US National Science Foundation grant DMR-2210083 (A.J.), DMR- 2215191 (O.D.L., digital holographic microscopy studies), and ECCS-2122399 (O.D.L., analysis of switching). The material FNLC 919 was provided by Merck Electronics KGaA, Darmstadt, Germany.

5. References

[1] Y. Choi, H. R. Kim, K. H. Lee, Y. M. Lee, and J. H. Kim, *A Liquid Crystalline Polymer Microlens Array with Tunable Focal Intensity by the Polarization Control of a Liquid Crystal Layer*, Appl Phys Lett **91**, 221113 (2007).

[2] J. F. Algorri, N. Bennis, V. Urruchi, P. Morawiak, J. M. Sánchez-Pena, and L. R. Jaroszewicz, *Tunable Liquid Crystal Multifocal Microlens Array*, Sci Rep **7**, 17318 (2017).

[3] Y. Zhang, X. Weng, P. Liu, C. Wu, L. Sun, Q. Yan, X. Zhou, and T. Guo, *Electrically High-Resistance Liquid Crystal Micro-Lens Arrays with High Performances for Integral Imaging 3D Display*, Opt Commun **462**, 125299 (2020).

[4] J. B. Wu, S. B. Wu, and W. Hu, *Azimuthal Orientation Guided Topological Defect Evolution across the Nematic-Smectic Phase Transition*, Phys Rev B **108**, 224107 (2023).

[5] S. B. Wu, J. B. Wu, H. M. Cao, Y. Q. Lu, and W. Hu, *Topological Defect Guided Order Evolution across the Nematic-Smectic Phase Transition*, Phys Rev Lett **130**, 078101 (2023).

[6] J. B. Wu, S. B. Wu, H. M. Cao, Q. M. Chen, Y. Q. Lu, and W. Hu, *Electrically Tunable Microlens Array Enabled by Polymer-Stabilized Smectic Hierarchical Architectures*, Adv Opt Mater **10**, 2201015 (2022).

[7] P. Popov, L. W. Honaker, M. Mirheydari, E. K. Mann, and A. Jákli, *Chiral Nematic Liquid Crystal Microlenses*, Sci Rep **7**, 1603 (2017).

[8] Y. Li, Y. Liu, and D. Luo, *A Photo-Switchable and Photo-Tunable Microlens Based on Chiral Liquid Crystals*, J Mater Chem C Mater **7**, 15166 (2019).

[9] G. Horváth, *Polarized Light and Polarization Vision in Animal Sciences, Second Edition* (2014).

[10] G. Horváth, G. Kriska, P. Malik, and B. Robertson, *Polarized Light Pollution: A New Kind of Ecological Photopollution*, Front Ecol Environ **7**, 317 (2009).

[11] B. Bernáth, G. Szedenics, H. Wildermuth, and G. Horváth, *How Can Dragonflies Discern Bright and Dark Waters from a Distance? The Degree of Polarisation of Reflected Light as a Possible Cue for Dragonfly Habitat Selection*, Freshw Biol **47**, 1707 (2002).

[12] T. Heinloth, J. Uhlhorn, and M. F. Wernet, *Insect Responses to Linearly Polarized Reflections: Orphan Behaviors without Neural Circuits*, Front Cell Neurosci **12**, 1 (2018).

[13] G. H. Brown and J. J. Wolken, *Liquid Crystals and Biological Structures* (Academic Press, New York, 1979).

[14] K. Perera, H. N. Padmini, E. Mann, and A. Jákli, *Polymer Stabilized Paraboloid Liquid Crystal Microlenses with Integrated Pancharatnam–Berry Phase*, Adv Opt Mater **2101510**, 1 (2021).

[15] K. Perera, N. Haputhantrige, S. Hossain, M. Mostafa, A. Adaka, E. Mann, O. D. Lavrentovich, and A. Jákli, *Electrically Tunable Polymer Stabilized Chiral Ferroelectric Nematic Liquid Crystal Microlenses*, Adv Opt Mater 2302500 (2023).

[16] X. Zhao, J. Zhou, J. Li, J. Kougo, Z. Wan, M. Huang, and S. Aya, *Spontaneous Helielectric Nematic Liquid Crystals: Electric Analog to Helimagnets*, Proceedings of the National Academy of Sciences USA **118**, e2111101118 (2021).

[17] H. Nishikawa and F. Araoka, *A New Class of Chiral Nematic Phase with Helical Polar Order*, Advanced Materials **33**, 2101305 (2021).

[18] C. Feng, R. Saha, E. Korblova, D. Walba, S. N. Sprunt, and A. Jákli, *Electrically Tunable Reflection Color of Chiral Ferroelectric Nematic Liquid Crystals*, Adv Opt Mater 2101230 (2021).

[19] J. Ortega, C. L. Folcia, J. Etxebarria, and T. Sierra, *Ferroelectric Chiral Nematic Liquid Crystals: New Photonic Materials with Multiple Bandgaps Controllable by Low Electric Fields*, Liq Cryst **49**, 2128 (2022).

[20] D. Pociecha et al., *Intrinsically Chiral Ferronematic Liquid Crystals: An Inversion of the Helical Twist Sense at the Chiral Nematic – Chiral Ferronematic Phase Transition*, J Mol Liq **361**, 119532 (2022).

[21] M. Born, *Über Anisotrope Flüssigkeiten. Versus Einer Theorie Der Flüssigen Kristalle Und Des Elektrischen Kerr-Effekts in Füssigkeiten*, Sitzungsber. Preuss Akad. Wiss **30**, 614 (1916).

[22] H. Nishikawa, K. Shiroshita, H. Higuchi, Y. Okumura, Y. Haseba, S. I. Yamamoto, K. Sago, and H. Kikuchi, *A Fluid Liquid-Crystal Material with Highly Polar Order*, Advanced Materials **29**, 1702354 (2017).

[23] R. J. Mandle, S. J. Cowling, and J. W. Goodby, *A Nematic to Nematic Transformation Exhibited by a Rod-like Liquid Crystal*, Physical Chemistry Chemical Physics **19**, 11429 (2017).

[24] X. Chen et al., *First-Principles Experimental Demonstration of Ferroelectricity in a Thermotropic Nematic Liquid Crystal: Polar Domains and Striking Electro-Optics*, Proc Natl Acad Sci U S A **117**, 14021 (2020).

[25] N. Sebastián, L. Cmok, R. J. Mandle, M. R. De La Fuente, I. Drevenšek Olenik, M. Čopič, and A. Mertelj, *Ferroelectric-Ferroelastic Phase Transition in a Nematic Liquid Crystal*, Phys Rev Lett **124**, 037801 (2020).

[26] N. Sebastián, M. Čopič, and A. Mertelj, *Ferroelectric Nematic Liquid Crystalline Phases*, Phys Rev E **106**, 021001 (2022).

[27] R. Saha, P. Nepal, C. Feng, M. S. Hossain, M. Fukuto, R. Li, J. T. Gleeson, S. Sprunt, R. J. Twieg, and A. Jákli, *Multiple Ferroelectric Nematic Phases of a Highly Polar Liquid Crystal Compound*, Liq Cryst **49**, 1784 (2022).

[28] M. T. Máthé, Á. Buka, A. Jákli, and P. Salamon, *Ferroelectric Nematic Liquid Crystal Thermo-Motor*, Phys Rev E **105**, L052701 (2022).

[29] K. Thapa, O. S. Iadlovska, B. Basnet, H. Wang, A. Paul, J. T. Gleeson, and O. D. Lavrentovich, *Confinement and Magnetic-Field Effect on Chiral Ferroelectric Nematic Liquid Crystals in Grandjean-Cano Wedge Cells*, Phys Rev E **109**, 054702 (2024).

[30] J.-S. Yu, J. H. Lee, J.-Y. Lee, and J.-H. Kim, *Alignment Properties of a Ferroelectric Nematic Liquid Crystal on the Rubbed Substrates*, Soft Matter **19**, 2446 (2023).

[31] M. T. Máthé, K. Perera, Á. Buka, P. Salamon, and A. Jákli, *Fluid Ferroelectric Filaments*, Advanced Science 202305950 (2023).

[32] M. T. Máthé, M. S. H. Himel, A. Adaka, J. T. Gleeson, S. Sprunt, P. Salamon, and A. Jákli, *Liquid Piezoelectric Materials: Linear Electromechanical Effect in Fluid Ferroelectric Nematic Liquid Crystals*, Adv Funct Mater 2314158 (2024).

[33] A. Jákli, O. D. Lavrentovich, and J. V. Selinger, *Physics of Liquid Crystals of Bent-Shaped Molecules*, Rev Mod Phys **90**, 045004 (2018).

[34] A. Mertelj, L. Cmok, N. Sebastián, R. J. Mandle, R. R. Parker, A. C. Whitwood, J. W. Goodby, and M. Čopič, *Splay Nematic Phase*, Phys Rev X **8**, 041025 (2018).

[35] X. Chen et al., *The Smectic ZA Phase: Antiferroelectric Smectic Order as a Prelude to the Ferroelectric Nematic*, Proc Natl Acad Sci U S A **120**, e2217150120 (2023).

[36] M. T. Máthé, Á. Buka, A. Jákli, and P. Salamon, *Ferroelectric Nematic Liquid Crystal Thermomotor*, Phys Rev E **105**, L052701 (2022).

[37] K. Perera, R. Saha, P. Nepal, R. Dharmarathna, M. S. Hossain, M. Mostafa, A. Adaka, R. Waroquet, R. J. Twieg, and A. Jákli, *Ferroelectric Nematic Droplets in Their Isotropic Melt*, Soft Matter **19**, 347 (2023).

[38] J. Li, Z. Wang, M. Deng, Y. Zhu, X. Zhang, R. Xia, Y. Song, Y. Hisai, S. Aya, and M. Huang, *General Phase-Structure Relationship in Polar Rod-Shaped Liquid Crystals: Importance of Shape Anisotropy and Dipolar Strength*, Giant **11**, 100109 (2022).

[39] K. Perera, R. Saha, P. Nepal, R. Dharmarathna, M. S. Hossain, M. Mostafa, A. Adaka, R. Waroquet, R. J. Twieg, and A. Jákli, *Ferroelectric Nematic Droplets in Their Isotropic Melt*, Soft Matter **19**, 347 (2022).

[40] X. Chen et al., *First-Principles Experimental Demonstration of Ferroelectricity in a Thermotropic Nematic Liquid Crystal: Polar Domains and Striking Electro-Optics*, Proc Natl Acad Sci USA **117**, 14021 (2020).

[41] P. Popov, L. W. Honaker, M. Mirheydari, E. K. Mann, and A. Jákli, *Chiral Nematic Liquid Crystal Microlenses*, Sci Rep **7**, 1603 (2017).

[42] Y.-H. Lin, Y.-J. Wang, and V. Reshetnyak, *Liquid Crystal Lenses with Tunable Focal Length*, Liq Cryst Rev **5**, 111 (2017).

[43] P. G. De Gennes, SOUS CHAMP MAGNETIQUE, Pergamon Press, 1970.

[44] N. V. Madhusudana and K. R. Sumathy, *Networks of Point Disclinations at the Nematic-Isotropic Iinterface*, Molecular Crystals and Liquid Crystals, Letters **92**, 193 (1983).

[45] A. J. Ferris, C. Rosenblatt, and T. J. Atherton, *Spontaneous Anchoring-Mediated Topography of an Orientable Fluid*, Phys Rev Lett **126**, 057803 (2021).

[46] V. Designolle, S. Herminghaus, T. Pfohl, and C. Bahr, *AFM Study of Defect-Induced Depressions of the Smectic-A/Air Interface*, Langmuir **22**, 363 (2006).

[47] G. Babakhanova, T. Turiv, Y. Guo, M. Hendrikx, Q. H. Wei, A. P. H. J. Schenning, D. J. Broer, and O. D. Lavrentovich, *Liquid Crystal Elastomer Coatings with Programmed Response of Surface Profile*, Nat Commun **9**, 456 (2018).

[48] P. Kumari, B. Basnet, M. O. Lavrentovich, and O. D. Lavrentovich, *Chiral Ground States of Ferroelectric Liquid Crystals*, Science (1979) **383**, 1364 (2024).